Advances in Bridge Engineering

ORIGINAL INNOVATION

Open Access

Entire mechanical analysis of prestressed CFRP strengthened RC beams under different prestressed introduced methods

Zhao-jun Zhang[1], Wen-wei Wang[2*], Jing-shui Zhen[1], Bo-cheng Li[1], De-cheng Cai[1] and Yang-yang Du[1]

*Correspondence:
wangwenwei@seu.edu.cn

[1] Offshore Oil Engineering Co., Ltd., Tianjin 300461, China
[2] Department of Bridge Engineering, School of Transportation, Southeast University, Nanjing 211189, China

Abstract

In order to clarify the effect of mechanical tensioning and SMA wire heating recovery on introducing prestress into CFRP sheet strengthened reinforced concrete (RC) beams, an experimental research on the bending performance of prestressed CFRP sheet strengthened RC beams was conducted. Based on the test results, a bending carrying capacity model for RC beams externally strengthened with prestressed CFRP sheets was proposed. The model provides calculation methods for the decompression moment, cracking moment, yielding moment, and ultimate moment, corresponding to different failure modes of the RC beams strengthened with externally bonded prestressed CFRP sheets. Four experimental beams were designed to verify the accuracy of the model with the prestresses of 100 MPa and 200 MPa. The results show that during the yield stage and strengthening stage, the loading-unloading stress-strain relationship curves of SMA wire under different prestrains are basically consistent. When the prestrain of SMA wire is 10%, the maximum recovery stress reaches 448.5 MPa. Under the same prestrain conditions, the maximum recovery stress of CFRP sheets was reduced by 37.8–39.5% when the prestress was introduced through heating recovery of SMA wires. The failure mode of mechanically tensioned prestressed CFRP sheet strengthened beams is the CFRP sheet debonding caused by mid-span bending cracks, while the failure mode of strengthened beams with prestressed CFRP sheet by SMA wire heating recovery is the CFRP sheet end debonding. The cracking moment and yield moment of the strengthened beams are significantly increased by two methods of introducing prestressing. The stiffness improvement of mechanically tensioned prestressed CFRP sheet strengthened beam is relatively large. While, the prestressed CFRP sheet strengthened beam by SMA wire heating recovery gradually experience end peeling failure of the CFRP sheet, and the prestressing effect does not effectively limit the development of cracks, resulting in limited stiffness improvement. The calculation results are in good agreement with the experimental results, proving that the proposed method for analyzing the entire bending process can be used to predict the bending mechanical properties of the prestressed CFRP sheet strengthened beams.

Keywords: Introduction method of prestressing, Prestressed CFRP sheet, Strengthening RC beams, Failure modes, Entire mechanical analysis

1 Introduction

Externally bonded Fiber Reinforced Polymer (FRP) sheet strengthening technology has been widely used in the reinforcement and repair of reinforced concrete (RC) structures (Derkowski and Walczak 2021). Despite the outstanding advantages of FRP, such as light weight, high strength, and good durability, this technology also has significant shortcomings (Wang 2007; Frigione and Lettieri 2018; Feng et al. 2011): (1) Low utilization rate of the strength of FRP sheet. The externally bonded FRP sheet strengthening technology is essentially a 'passive' reinforcement technology, and the FRP sheet obviously acts to load the force relatively late. Under normal use and limit states, its high-strength characteristics cannot be fully utilized. (2) It cannot effectively improve the service performance of the RC structure. For RC structures with cracks, sufficient external stress is needed to limit the development of the original cracks. The continuous development of cracks will lead to a sustained decrease in the stiffness of the structure. Using the non-prestressed CFRP sheet clearly cannot achieve the goal of limiting crack development and improving the stiffness of the structures (Basaran and Kalkan 2020; Zhang et al. 2015; Wang et al. 2013).

In order to address the aforementioned issues, some scholars have proposed introducing prestressing into FRP sheet to form the prestressed FRP sheet strengthening technology (Shi 2021; , Kueres et al. 2020), and have conducted extensive research on prestressed FRP sheet strengthened RC beams and RC columns (Tiwary et al. 2022; Hassan et al. 2021; Koteš et al. 2020). However, the existing prestressed FRP sheet strengthened technology still has some drawbacks: the procedure for applying the prestressing is cumbersome (for example, specialized tensioning and anchoring devices need to be designed, and sufficient operating space is required). Mechanical tensioning prestressed FRP sheets technology usually results in significant short-term prestress losses due to the short anchorage length (Wang et al. 2012; , Soleilhet et al. 2023), and it is difficult to apply prestressing in small spaces. Therefore, there is an urgent need to find an effective and direct technique to introduce prestresses into FRP sheets, in order to expand the application of the prestressed FRP sheets in engineering.

Previous research works (Hui et al. 2022; Xue et al. 2022; Xue et al. 2023) have proposed a technique that utilizes the shape memory effect of shape memory alloy (SMA) wires to introduce prestresses into FRP sheets by heating and recovering, and have conducted experimental research on the flexural and shear strengthening of RC beams using the prestressed carbon fiber reinforced polymer (CFRP) sheets. These research findings verified the effectiveness of introducing prestress with the SMA wire recovery effect. In order to further study the strengthening effect of the mechanical tensioning method and the SMA wire heating recovery method, this paper conducted flexural performance tests on the prestressed CFRP sheet strengthened RC beams under two prestress introduction methods, and established a full-process analysis method for the bending moments of the prestressed CFRP sheet strengthened RC beams.

2 Theoretical analysis framework

As mentioned earlier, regardless of the method used to introduce the prestress, the strengthened beam can be considered as a reinforcement technique using externally bonded prestressed FRP sheet, and therefore, an analysis model can be established according to the analysis method of the prestressed concrete beams. As shown in Fig. 1, a rectangular section beam strengthened with prestressed FRP sheet is subjected to the entire process of force, which is divided into the prestressing stage, the decompression stage under the external loads, the cracking stage, the yielding stage, and the failure stage. For ease of comparison and analysis, the stress and strain distributions on the vertical section in Fig. 1 are plotted on the same section, where the dashed lines represent the strain distribution and the solid lines represent the stress distribution.

1) Prestressing stage

In the prestressing stage, the prestress is introduced into FRP sheets through either mechanical tension or SMA wires by heating and recovering. However, the prestress losses will occur over time for both methods. According to the reports in reference (Soleilhet et al. 2023), the prestress losses in the mechanical tension method are mainly caused by the shrinkage and slip of the CFRP sheet, as well as the friction between the tensioning device and the CFRP sheet. The prestress losses usually account for 18.7% of the tensioning stress. While the prestress losses in the SMA wire method is mainly caused by the shrinkage of the CFRP sheet, and usually accounts for 9.5% of the tensioning stress (Xue et al. 2023). To simplify the calculation, this paper suggests that the prestress losses for two prestressing methods can be approximately calculated by the following equation:

$$\sigma_1 = \begin{cases} 0.187\sigma_{con} & \text{Mechanical tensioning} \\ 0.095\sigma_{con} & \text{SMA wire recovery} \end{cases} \tag{1}$$

Where, σ_1 is the prestress losses; σ_{con} is the tensioning stress. The effective prestress is defined as:

$$\sigma_{pe} = \sigma_{con} - \sigma_1 \tag{2}$$

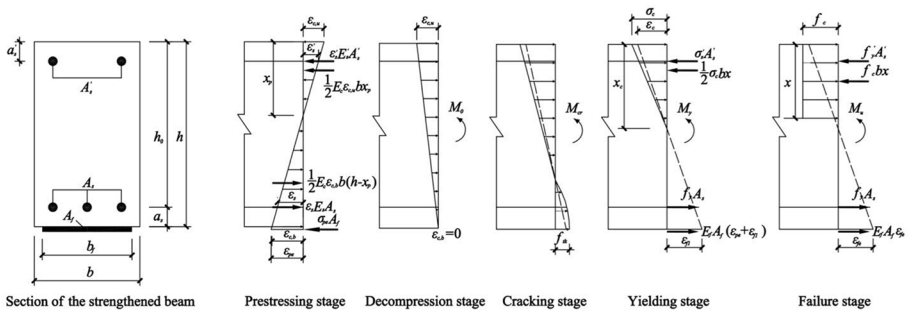

Fig. 1 Calculation model

Where σ_{pe} is the effective prestress after the prestress losses. During the pre-tensioning stage, the concrete beam is in an elastic state, and the strain distribution of the cross-section conforms to the assumption of a plane section. The stress-strain relationship of the material is linear. Under the action of the prestress, the concrete on the upper part of the beam is under tensile stress, while the concrete on the lower part is under compressive stress. According to the assumption of a plane section, it can be obtained that:

$$\begin{cases} \epsilon_{c,u} = \frac{x_p}{h-x_p}\epsilon_{c,b} \\ \epsilon_s = \frac{x_p}{h_0-x_p}\epsilon_{c,b} \\ \epsilon_s' = \frac{x_p}{a_s'}\epsilon_{c,b} \end{cases} \tag{3}$$

Where, $\epsilon_{c,b}$ represents the precompression strain of the concrete at the lower edge of the beam; $\epsilon_{c,u}$ represents the pretension strain of the concrete at the upper edge of the beam; ϵ_s is the strain of the tensile steel reinforcement; ϵ_s' is the strain of the compressive steel reinforcement; x_p is the height of the compressed concrete zone during the pressure release stage; h is the height of RC beam; and a_s' is the distance from the centroid of the compressive steel reinforcement to the top surface of the beam.

Based on the force on the beam section and the bending moment equilibrium at the point of action of the resultant force on the tensile zone of the concrete, it can be obtained that:

$$\frac{1}{2}E_c\epsilon_{c,u}bx_p + \sigma_{pe}A_f + E_s'\epsilon_s'A_s{}' = \frac{1}{2}E_c\epsilon_{c,b}b(h-x_p) + E_s\epsilon_sA_s \tag{4}$$

$$\frac{1}{3}E_c\epsilon_{c,b}bh(h-x_p) + E_s\epsilon_sA_s\left(h_0-\frac{x_p}{3}\right) = \sigma_{pe}A_f\left(h-\frac{x_p}{3}\right) + E_s'\epsilon_s'A_s{}'(a_s{}'-\frac{x_p}{3}) \tag{5}$$

In the equations, A_s, $A_s{}'$, A_f represents the cross-sectional area of the tensile reinforcement, the cross-sectional area of the compressive reinforcement, and the area of the CFRP sheet, respectively; b is the width of RC beam; E_s, E_s', and E_c represent the elastic moduli of the tensile reinforcement, compressive reinforcement, and concrete, respectively.

By solving Eqs. (2) to (5) simultaneously, assuming a precompression strain of the concrete $\epsilon_{c,b}$, the compressed height x_p of the concrete can be obtained through the iterative method.

2) Decompression state

The decompression state refers to the condition in which the concrete at the bottom of the beam is under tension due to the external load (external bending moment), which counteracts the precompression strain and making $\epsilon_{c,b} = 0$:

$$\epsilon_{c,b} - \frac{M_0}{W_0E_c} = 0 \tag{6}$$

By rearranging Eq. (6), we can obtain:

$$M_0 = W_0 E_c \epsilon_{c,b} \tag{7}$$

Where, M_0 represents decompression bending moment; W_0 represents flexural modulus of the transformed section of the entire cross-section for the strengthened beam, $W_0 = \frac{I_0}{h-x_p}$; I_0 represents effective moment of inertia of the transformed section of the entire cross-section for the strengthened beam. For the sake of simplifying calculations, the transformed section of the CFRP sheet may be neglected when calculating the characteristics of the entire cross-section.

3) Cracking moment

As the external load increases, the tensile stress in the concrete at the tension edge of the beam gradually increases to the tensile strength of the concrete, corresponding to the cracking moment which is defined as:

$$M_{cr} = \gamma_0 f_{tk} W_0 + M_0 \tag{8}$$

Where, M_{cr} is the cracking moment; f_{tk} is the tensile strength of concrete; γ_0 is the plasticity influence factor.

4) Yield stage

The yield stage mainly determines the yield moment. At this point, the beam has already cracked, the tensile steel bars have yielded, but the compressive zone concrete strain is less than 0.002, and the concrete stress is distributed in a triangular manner. By the force equilibrium, we can obtain:

$$\frac{1}{2}\sigma_c b x_c + \sigma'_s A'_s = f_y A_s + E_f A_f \left(\epsilon_{pf} + \epsilon_{f1}\right) \tag{9}$$

Where, σ_c is the compressive stress in the concrete at the compression edge, $\sigma_c = E_c \epsilon_c$; ϵ_c is the compressive strain in the concrete at the compression edge; σ'_s is the compressive stress in the steel reinforcement, $\sigma'_s = E'_s \epsilon'_s$; ϵ'_s is the compressive strain in the steel reinforcement; x_c is the height of the compressed zone of concrete; f_y is the yield strength of the tensile steel reinforcement; E_f is the elastic modulus of the CFRP sheet; ϵ_{pf} is the prestress strain in the CFRP sheet corresponding to the effective stress; ϵ_{f1} represents is the additional strain of the CFRP sheet after loading.

Based on the assumption of a plane section, we can calculate ϵ'_s and ϵ_{f1}:

$$\begin{cases} \epsilon_{f1} = \frac{h-x_c}{x_c}\epsilon_c \\ \epsilon'_s = \frac{x_c - a'_s}{x_c}\epsilon_c \end{cases} \tag{10}$$

By simultaneously solving Eqs. (9) and (10) using an iterative method, we can obtain the height of the compressed concrete zone x_c.

By taking the moment of the point of the resultant force acting on the compressed concrete zone, the yielding moment can be obtained:

$$M_y = E_f A_f (\epsilon_{pf} + \epsilon_{f1}) \left(h - \frac{x_c}{3}\right) + f_y A_s (h_0 - \frac{x_c}{3}) + \sigma_s' A_s' (a_s' - \frac{x_c}{3}) \quad (11)$$

Where, M_y is the yielding moment; h_0 is the effective height of the section, $h_0 = h - a_s$;a_s is the distance from the centroid of the tension steel reinforcement to the bottom edge of the beam.

5) Failure stage

In the failure stage, the ultimate moment is reached. For the strengthened beam, failure typically occurs through the crushing of the compressed concrete after yielding of the tension steel reinforcement, the fracture of CFRP sheets after yielding of the tension steel reinforcement, the debonding of CFRP sheets caused by flexural cracks, and the end debonding of CFRP sheets. The failure mode of CFRP sheet fracture can be limited by the condition of the relative critical compressed height. This study mainly considers the failure modes of compressed concrete crushing, CFRP debonding caused by flexural cracks (i.e., intermediate crack debonding, IC debonding), and CFRP end debonding (ED debonding). For the failure modes of compressed concrete crushing and IC debonding caused by flexural cracks, both the tension and compression steel reinforcements have yielded, and the stress distribution in the compressed concrete zone is nonlinear. The stress-strain relationship can be determined with reference to relevant codes and specifications (Ministry of Housing and Urban-Rural Development 2010; Ministry of Transport of the People's Republic of China 2018). To simplify the calculations, this study adopts the calculation model of an equivalent rectangular stress diagram.

As shown in Fig. 1, by the equilibrium of forces, we can derive:

$$f_c b x + f_y' A_s' = f_y A_s + E_f A_f \epsilon_{fe} \quad (12)$$

Where, f_c is the compressive strength of concrete; f_y and f_y' are yield strength of the tensile steel reinforcement and yield strength of the compression steel reinforcement, respectively; ϵ_{fe} is effective strain of CFRP sheets.

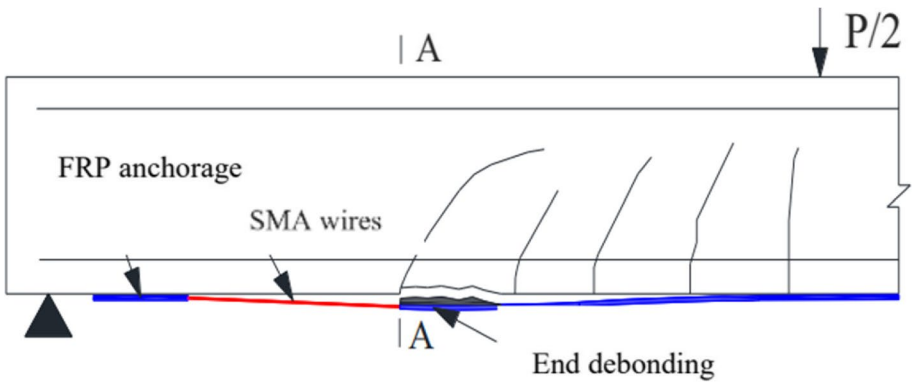

Fig. 2 The failure mode of end debonding of CFRP sheets

$$\varepsilon_{fe} = \begin{cases} \frac{(h-x)}{x}\varepsilon_{cu} & \text{concrete crushing} \\ 0.91\varepsilon_{cu} & \text{IC debonding} \end{cases} \tag{13}$$

In the case of end debonding of the CFRP sheets occurring at the location A-A section of the test beam, the debonding at that location is constrained by the SMA wire, as shown in Fig. 2. Therefore, the anchorage effect of the SMA wire and the prestressing effect of the CFRP sheets should be taken into account. To predict the ultimate load in this failure mode, the model proposed in reference (Teng and Yao 2007) was modified to accommodate the restrictive effect of the SMA wire on the end debonding of the CFRP sheets.

For the failure mode of end debonding, the debonding moment (Teng and Yao 2007) can be expressed as following:

$$M'_{db,f} = \frac{0.488M_{u,1}}{\left(\alpha'_{flex}\alpha'_{axial}\alpha'_{w}\right)^{1/9}} \tag{14}$$

Where, $M_{u,1}$ is the debonding moment at the end of the CFRP sheet (corresponding to the section A-A depicted in Fig. 2). Different from CFRP strengthening beams that introduce prestressing through mechanical tensioning, Eq. (14) considered the contribution of SMA wire to the flexural capacity; α'_{flex}, α'_{axial} and α'_{w} are applying correction factors, representing the influence of CFRP strengthening on flexural stiffness, the effect of axial stiffness ratio, and the impact of width ratio, respectively:

$$\alpha'_{flex} = \frac{EI_{cr,p} - EI_{cr}}{EI_{cr}} \tag{15}$$

Where, EI_{cr} is the flexural stiffness of the unstrengthened beam at the cracked section, $EI_{cr,p}$ is the flexural stiffness of the CFRP strengthening beam. The flexural stiffness can be calculated using the transformed section method for all cases.

$$\alpha'_{axial} = \frac{E_f t_f - E_{sm} t_{sm}}{E_c h_0} \tag{16}$$

Where, E_{sm} is the elastic modulus of SMA wire. t_{sm} is the equivalent thickness of SMA wire, $t_{sm} = nA_{sm}/b_f$; n is the number of SMA wires, A_{sm} is the cross-sectional area of a single SMA wire; t_f is the thickness of the CFRP sheets; b_f is the width of the CFRP sheets.

$$\alpha'_{w} = \frac{b}{b_f} \leq 3 \tag{17}$$

3 Experimental research

To validate the effectiveness of the established analysis method, this study conducted experimental tests on the flexural performance of RC beams strengthened with prestressed CFRP sheets using different induced prestressed methods.

3.1 The specimen design and material properties

A total of five simply supported reinforced concrete beams were designed for the experiment. One beam served as the control beam (CL) without any strengthening. Two beams, CF-100 and CF-200, were strengthened with two layers of prestressed CFRP sheets, with designed prestress of 100 MPa and 200 MPa obtained by mechanical tensioning method, respectively. The remaining two beams, SCF-100 and SCF-200, were strengthened with the prestressed CFRP sheets induced by SMA wires' recovery. The designed recovery stresses were also 100 MPa and 200 MPa, respectively, for comparison. The CFRP sheets consisted of two layers in both cases.

The experimental beams were rectangular in cross-section, with dimensions of length × width × height = 2000mm × 160mm × 280mm. The concrete used in the beams had a design strength grade of C40. Two longitudinal reinforcing rebars with a diameter of 16 mm were placed at the bottom of the beams, while two longitudinal reinforcing rebars with a diameter of 12 mm were arranged at the top. In the bending-shear regions, 8 mm diameter stirrups were uniformly spaced at a distance of 50 mm, while in the pure bending region, the stirrup spacing was set at 200 mm. All the reinforcing rebars used were HRB400 grade steel rebars, and they were securely tied together to form the reinforcement framework. The design of the experimental beams is illustrated in Fig. 3.

The design strength grade for concrete in the experiment is C40, and the mix proportion is as follows: cement: fine aggregate: coarse aggregate: water: admixture = 1: 1.29: 2.88: 0.39: 0.01. According to the provisions of the *Code for Design of Concrete Structures* (GB50010–2010), three standard cubic specimens with a side length of 150 mm were prepared using the standard method. The compressive strength of the concrete cubes at the age of 28 days was obtained. Additionally, three prismatic specimens with dimensions of 150 mm×150 mm×300 mm were prepared to measure the axial compressive strength and elastic modulus of the concrete. The concrete specimens were cured under the same humidity and temperature conditions as the strengthened RC beams, ensuring consistency with various parameters of the test beams. The measured compressive strength of the concrete cubes, axial compressive strength, and elastic modulus are shown in Table 1.

Three samples were randomly selected for each type of steel rebars to perform uniaxial tensile tests for obtaining the mechanical properties of the steel rebars. Including yield strength, ultimate tensile strength, and elongation, as shown in Table 1. The CFRP sheet

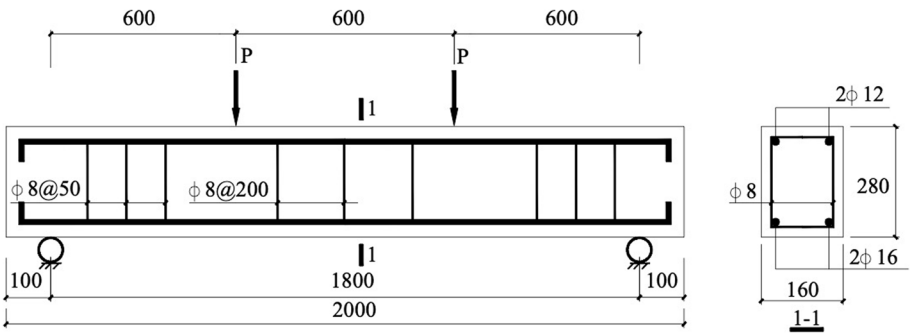

Fig. 3 Experimental beam design (unit in mm)

Table 1 Material properties

Material		Strength (MPa)				Elastic modulus(GPa)	Elongation(%)
		Cube compressive	Axial compression	Yield	Ultimate		
Concrete		39.6	40.5	-	-	38.6	-
Reinforcing steel rebar	16 mm	-	-	472	643	180	10.9
	12 mm	-	-	498	588	164	11.5
	8 mm	-	-	538	633	155	18.0
CFRP sheet		-	-	-	2804	209.4	1.49
SMA wire	1 mm	-	-	112.8	918.4	-	61.2

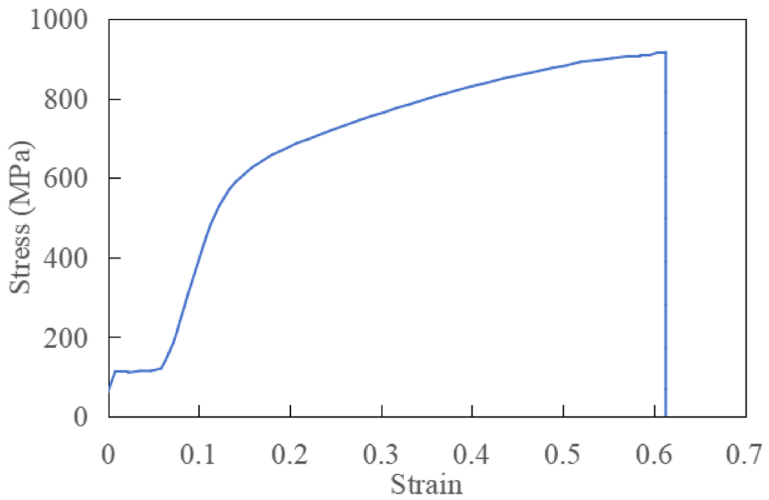

Fig. 4 The stress-strain curve of the SMA wire

used was CFS-I-300 type produced by Caben Composite Materials (Tianjin) Co., Ltd., which was impregnated with epoxy resin. The CFRP sheet specimens were 25 mm wide and 250 mm long for mechanical performance. To facilitate clamping, aluminum plates with a size of 50 mm×25 mm×2 mm were pasted on both ends of the CFRP sheets using epoxy resin. The specimens were subjected to tensile tests after cured for 7 days. The measured mechanical properties of the CFRP sheets are shown in Table 1.

The SMA material used in the experiment was the 1 mm-diameter Ni-Ti alloy wire produced by Xi'an Saite Metal Materials Development Co., Ltd. Prior to testing the mechanical properties, differential scanning calorimetry was used to perform phase transition temperature testing. The martensitic transformation start temperature M_s and finish temperature M_f were found to be 35.81°C and 59.00°C, respectively, while the austenitic transformation start temperature AT_s and finish temperature AT_f were found to be 73.19°C and 105.45°C, respectively. The laboratory temperature range was between 5°C and 20°C, which is below the austenitic transformation start temperature and thus effectively utilized the shape memory effect of the SMA material.

The displacement-controlled method was applied, and the loading speed of the SMA wire was 2 mm/min, and the experimental temperature was 8.7°C. The stress-strain curve obtained from the experiment is shown in Fig. 4. It can be seen from the

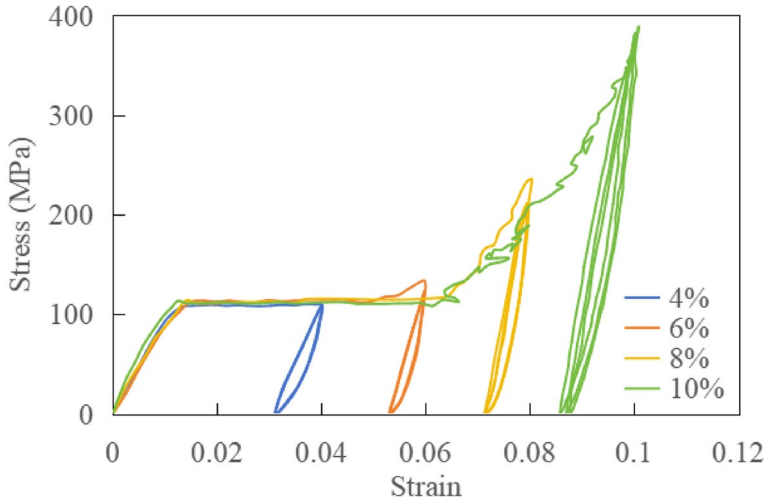

Fig. 5 The loading-unloading curves of the SMA material under different prestrain level

Table 2 Recovery stress and residual strain of SMA wires

Number		Prestrain%	Residual strain%	Recovery stress (MPa)
SMA wires	1	4	3.15	260.0
	2	6	5.34	306.3
	3	8	7.21	383.9
	4	10	8.73	448.5
SMA-CFRP	1	6	-	185.2
	2	8	-	238.6

figure that the SMA wire entered the yield stage at a stress of 112.8 MPa, with a yield plateau of approximately 6%. Subsequently, it entered the strengthening stage, and the stress level rapidly increased until fracture occurred. The corresponding ultimate strength was 918.4 MPa, with an elongation of 61.2%.

To obtain the shape memory effect of the SMA wire, it is necessary to stretch it to a certain strain and then unload before applying an electrical current to heat it up for recovery. With the temperature increasing, the SMA wire exhibits a recovery effect and can essentially return to its original length under an unconstrained state. If the SMA wires are constrained at its two ends, a certain amount of recovery stress is generated due to the stress balance conditions. The experiment was designed with four different initial strain levels of 4%, 6%, 8%, and 10%. After stretching to the designated initial strain level, the SMA wire was subjected to loading-unloading cycles three times to eliminate residual plastic deformation. The displacement-controlled method was applied, and the loading rate was 2.0 mm/min. The unloading rate was 1.0 mm/min.

In addition, a group of SMA wire specimens with the same initial strain level were also set up to test the maximum recovery stress under constrained conditions at both ends. It should be noted that simply heating the SMA wires after stretching it and

keeping it in a deformed state does not generate the required recovery force. Only after being stretched to a certain prestrain level, relaxed, and then subjected to constrained conditions with a certain amount of residual deformation at both ends, the wires can generate recovery stress by heating. The measured residual strain and maximum recovery stress are shown in Table 2.

Figure 5 shows the stress-strain hysteresis curves of the SMA wire under loading-unloading cycles at different prestrain levels. It can be seen from the figure that the shape of the stress-strain hysteresis curve during the yield and strengthening stages is basically the same after loading-unloading cycles, and the residual strain after complete unloading remains consistent. Based on the experimental data, the residual strain and corresponding recovery stress at each prestrain level are obtained and shown in Table 2.

Figure 6 presents the relationship curves between the prestrain of the SMA wire and the recovery stress and residual strain. Based on the relationship curves established in Fig. 6, the regression test data can be used to obtain the equation that describes the relationship between the prestrain, recovery stress, and residual strain:

$$\epsilon_r = 0.93\epsilon_p - 0.41 \tag{18}$$

$$\sigma_{r.max} = \begin{cases} 1.14\epsilon_p^2 + 16.14\epsilon_p + 174.92 \\ 3.17\epsilon_r^2 - 3.26\epsilon_r + 237.65 \end{cases} \tag{19}$$

Where, ϵ_p is the prestrain of SMA wire (%), ϵ_r is the residual strain of SMA wire (%), $\sigma_{r.max}$ is the maximum recovery stress of SMA wire (MPa).

3.2 Experimental equipment

3.2.1 Mechanical tensioning

In order to apply prestress to the CFRP sheets, a displacement self-constrained tensile equipment was designed, as shown in Fig. 7. The tensioning equipment consists of an

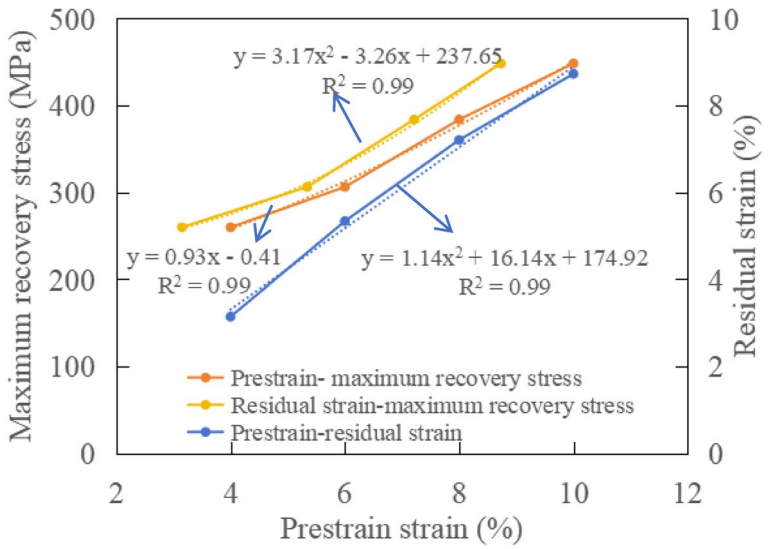

Fig. 6 The regression of maximum recovery stress

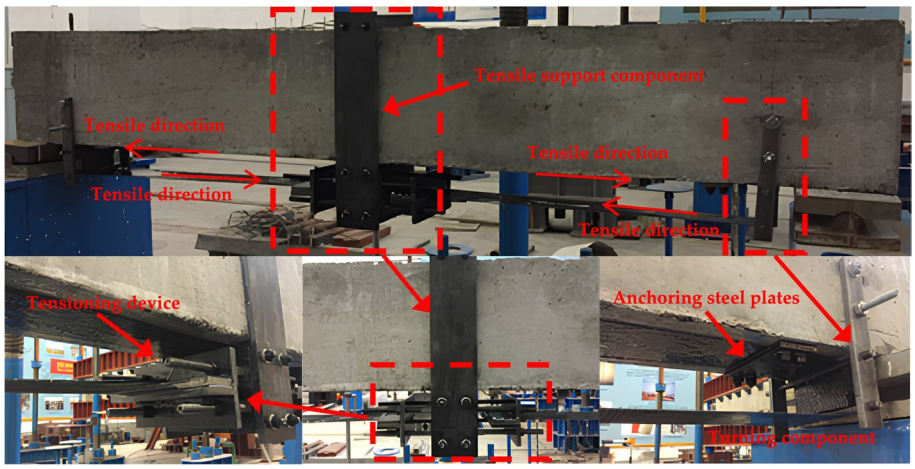

Fig. 7 Mechanical tensioning equipment for prestressed CFRP sheets

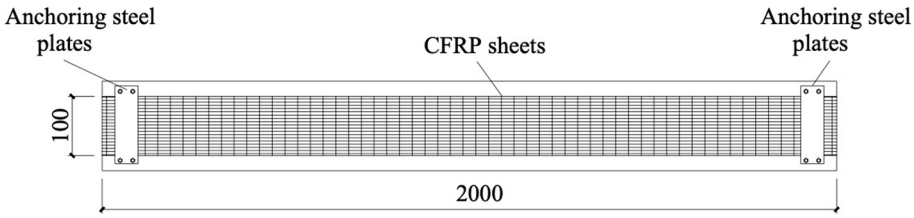

Fig. 8 Layout of the prestressed CFRP sheets under mechanical tensioning test (unit in mm)

tensioning device, a tensile support component and two turning components. The tensioning device is a T-shaped steel component, located on both sides of the tensile support component. The horizontal steel plate of the T-shaped component clamps the CFRP sheets, and by tightening the nuts on the four screws, and the vertical steel plate moves towards the mid span direction of the beam to tension the CFRP sheets and obtain prestress. The tensile support component is located in the middle of the test beam, while the turning component and the anchoring steel plates are located at the two ends of the test beam. The tensile support component is composed of two steel plates, i.e. the front steel plate and the rear steel plate. The front steel plate and the rear steel plate are respectively set on the two sides of the beam, and are connected by bolts through transverse steel plates on the top surface of the beam.At the same time, their lower parts are connected to the tensioning device with bolts to fix the tensioning device. The turning components are anchored near the end of the beam and consists of two rollers on top and bottom to turn the CFRP sheets from the bottom of the beam to the tensioning device.

The processes of applying the prestressing to the CFRP sheets by the mechanical tensioning method are as follows: (1) Fixing the turning components, anchoring steels, and tensile support component in the corresponding positions on the test beam according to the design scheme. (2) Pasting the CFRP sheets coated with epoxy resin on the bottom surface of the test beam, and connect the two ends to the tensioning device of the tensile support component through the rollers of the turning component, respectively. (3) After the tensioning device clamps the CFRP sheets, tightening the CFRP sheets by rotating

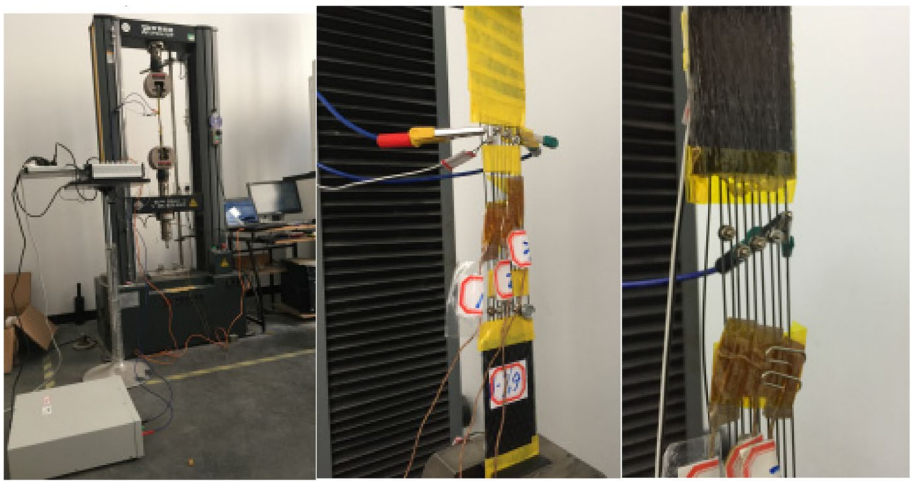

Fig. 9 Introducing prestress in CFRP sheets by heating the parallel SMA wires

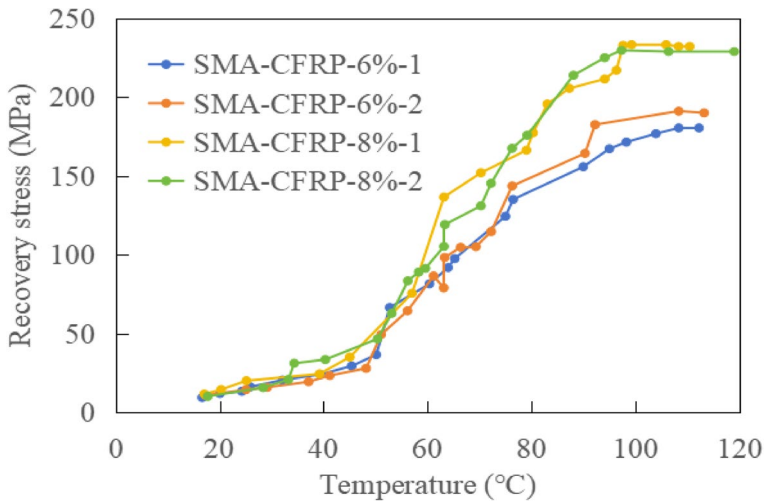

Fig. 10 Temperature-recovery stress curves of SMA-CFRP at different prestrain levels

the four nuts simultaneously to apply the prestress. (4) When the design tension stress is reached, anchoring the two ends of the CFRP sheets to the bottom surface of the beam at both ends through the anchoring steel plates, thus forming a prestressed CFRP sheets system, as shown in Fig. 8.

3.2.2 Introducing prestress through SMA wire heating and recovery

Another method of introducing prestress in this study is through the recovery of SMA wires upon heating. Similar to the SMA wire recovery performance test, the SMA wires were combined with CFRP sheets to test the effect of introducing prestress through the simultaneous recovery of multiple SMA wires. The temperature of the SMA wires was controlled by electric current, with an interval of 0.5 A for heating. Ten SMA wires were arranged in parallel and connected in an 'S' shape using bolts to ensure that the current was the same for each wire, as shown in Fig. 9. Based on the recovery stress test results

of a single SMA wire, the recovery stress was relatively small at a prestrain level of 4%. Therefore, this experiment only tested the recovery stress of SMA wires with prestrain levels of 6% and 8% in CFRP sheets.

Figure 10 shows the measured temperature-recovery stress curves for parallel SMA wires. As can be seen from this figure, similar to a single SMA wire, the recovery stress-temperature curve generally shows an 'S' shaped trend: as the temperature increasing, the recovery stress gradually increases, and when the temperature reaches above 110°C, the recovery stress reaches its maximum value, with the measured data shown in Table 2. However, compared with the recovery stress of a single SMA wire, the introduction of prestress in the CFRP sheets at prestrain levels of 6% and 8% resulted in a reduction of 39.5% and 37.8%, respectively. This is because the recovery effects of multiple SMA wires affect each other, and when the stress level is high, cracking occurs at the edges due to the low tensile strength of the epoxy resin adhesive, causing partial debonding of the SMA wires and leading to stress relaxation.

The strengthening details of the test beam introduced the prestressing through SMA wire heating and recovery is divided into two zones: the composite zone and the active zone (as shown in Fig. 11). The composite zone consists of embedding SMA wires into the CFRP sheets with a embedded length of 100 mm and has a total length of 400 mm. The active zone consists of parallel-setting SMA wires, which are used to introduce prestress into the CFRP sheets in the composite zone through the heating and recovery effect of SMA wires, as shown in Fig. 11. The SMA wires have a diameter of 1.0 mm, and the CFRP sheets have a width of 100 mm. Steel plates were used to anchor CFRP sheets near the beam supports in the composite zone. The manufacturing process of the composite zone is as follows: first, a layer of CFRP sheet was laid on the bottom face of the test beam, and then a layer of epoxy resin was painted evenly on the CFRP sheet. Then, the SMA wires were arranged on the CFRP sheet with a spacing of 3 mm, and another layer of CFRP sheet was covered with epoxy resin. After the epoxy resin is completely cured, the SMA wires with prestrain were heated and recovered to obtain recovery stress.

4 Result analysis

4.1 The failure modes and load-displacement curves

The failure mode of the CL beam is a typical bending failure, where the concrete in the compressed zone is crushed after the yielding of the tensile reinforcement, as shown in Fig. 12a). The failure mode of the prestressed CFRP sheets strengthened beams by mechanical tensioning CF-100 and CF-200 is the debonding of CFRP sheets caused by the bending cracks (i.e., IC debonding) and the subsequent fracture of the CFRP sheets, as shown in Fig. 12b). The failure mode of the SMA-introduced prestressed CFRP sheets

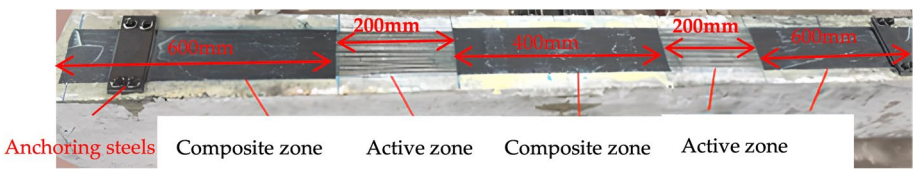

Fig. 11 Introducing prestress into SMA wires

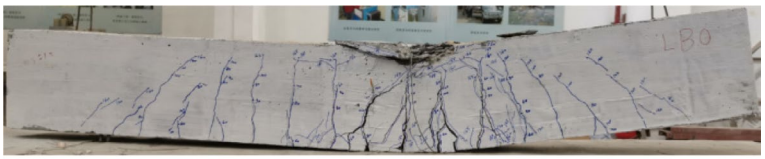

(a) Concrete crushing in the compressed zone

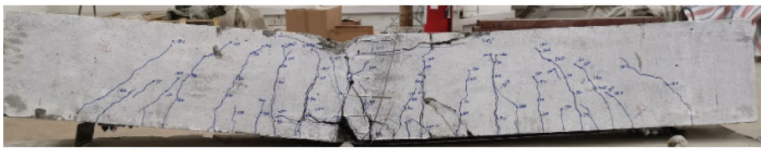

(b) IC debonding of CFRP sheets

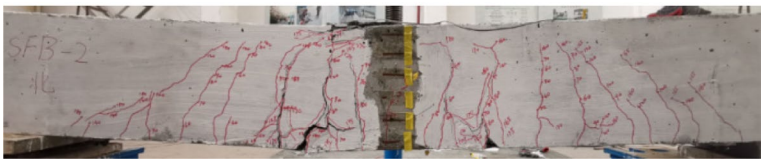

(c) End debonding of CFRP sheets of the composite zone

Fig. 12 Test failure mode

strengthening beam is the end debonding of the CFRP sheets of the composite zone, as shown in Fig. 12c).

The test beams CF-100 and CF-200 are the CFRP sheets strengthening beams with prestresses of 100 MPa and 200 MPa applied by mechanical tensioning, respectively. For the sake of simplicity, only the load development process of the CF-100 test beam is described here. When loaded to 36 kN, a vertical crack with a width of 0.04 mm and a length of about 34 mm appeared in the concrete at the lower edge of the beam under the loading point. When loaded to 60 kN, diagonal cracks appeared in the shear-span region. When loaded to 80 kN, the bending cracks extended up to the top surface of the beam and the width continued to develop, while new bending cracks appeared. When loaded to 140 kN, the crack width suddenly widened to 0.26 mm, and the beam emitted a loud 'pop' sound. When loaded to 180 kN, the crack continued to widen, and the CFRP sheets peeled off at the crack near at the mid-span position. When loaded to 200 kN, the CFRP sheets continued to peel off towards the support direction. When loaded to 208 kN, the middle section of the CFRP sheet completely debonded from the concrete, and the concrete in the compressed zone was crushed after the CFRP sheets fracture.

Figure 13 shows the load-displacement curves of all test beams. It can be seen from the figure that the load-displacement curves of the test beams can be divided into three stages: the un-cracking stage, the cracked-yield stage, and the yielded-failure stage. Before concrete cracking, the load-displacement curves are basically the same, indicating that the CFRP sheets have limited effect on the stiffness improvement of the strengthened beams. After cracking, the strengthened beams with the prestressed CFRP sheets introduced by mechanical tensioning show significant stiffness improvement, while the stiffness improvement of the strengthened beams with the prestressed CFRP sheets introduced by the recovery of SMA wires is limited.

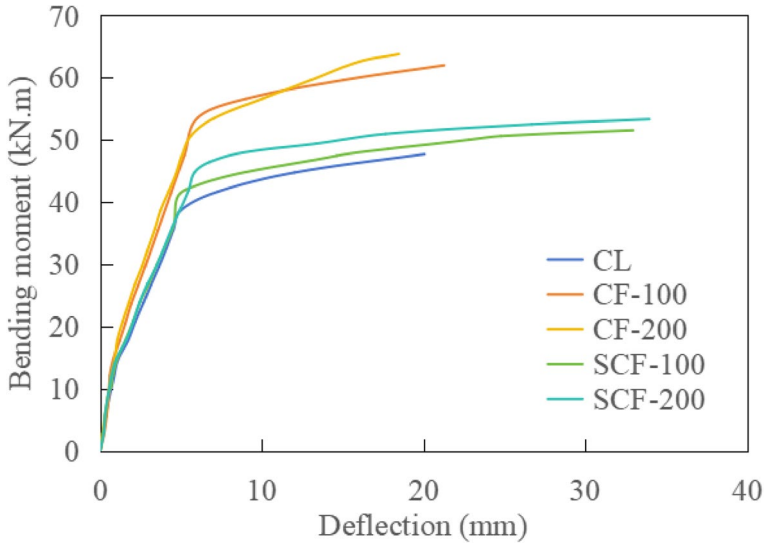

Fig. 13 The load-deflection curves of the test beams

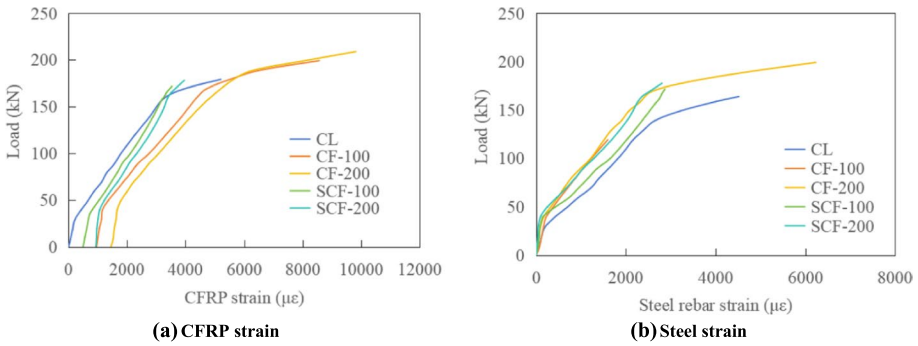

Fig. 14 Load-strain curves of the test beams

The reason is that the relatively small length of the composite zone is unable to suppress the development of cracks. Therefore, there was no significant change in the stiffness of the strengthened beam compared to the control beam. In practical engineering applications, the length of the composite zone should be increased as much as possible.

Compared with the yield load and ultimate load, there is also a significant difference in the degree of improvement between the two methods of introducing prestress. The mechanical tensioning method shows a higher ratios of improvement in both yield load and ultimate load, with an average increase of 26.5% and 25.6%, respectively. In comparison, under the prestress introduced by the recovery of SMA wires, the yield load and ultimate load were increased by an average of 17.3% and 6.7%, respectively, which is relatively low. The reason is that the end of the CFRP sheets experienced debonding failure, and the material properties were not fully utilized.

Table 3 Design of the test beams

Specimen name	Design of prestressing levels	Introducing prestressing methods	CFRP sheet prestrain (με)	CFRP sheet prestress (MPa)
CL	-	-	-	-
CF-100	100 MPa	Mechanically tensioned prestressed CFRP sheets, two-layered CFRP	480	100.5
CF-200	200 MPa		955	200.0
SCF-100	100 MPa	SMA wires recovered to introduce stress CFRP sheet, two-layered CFRP	491	102.8
SCF-200	200 MPa		929	194.5

Table 4 The characteristic test values of the test beams

Specimen name	$M_{cr}(kN \cdot m)$			Inc. (%)	$M_y(kN \cdot m)$			Inc. (%)	$M_u(kN \cdot m)$			Inc. (%)
	Exp.	Cal.	(1)		Exp.	Cal.	(2)		Exp.	Cal.	(3)	
CL	9.0	8.83	1.02	-	41.6	40.9	1.02	-	49.2	42.8	1.15	-
CF-100	10.8	9.62	1.12	20.0	52.8	47.6	1.11	26.9	62.4	57.5	1.09	26.8
CF-200	12.0	10.27	1.17	33.3	51.7	48.5	1.07	24.3	64.2	58.2	1.10	30.5
SCF-100	10.5	9.62	1.09	16.7	46.3	47.6	0.97	11.3	51.6	55.9	0.92	4.9
SCF-200	12.0	10.27	1.17	33.3	51.3	48.5	1.06	23.3	53.4	60.2	0.89	8.5
Ave.	-	-	1.14	-	-	-	1.06	-	-	-	1.03	-
COV	-	-	0.05	-	-	-	0.04	-	-	-	0.10	-

M_{cr}-cracking moment; M_y-yielding moment; Mu-ultimate moment; Exp.-experimental value; Cal.-calculated value; Inc.-increment ratio; (1)-ratio of the experimental value to the calculated value of the cracking moment; (2)-ratio of the experimental value to the calculated value of the yielding moment; (3)-ratio of the experimental value to the calculated value of the ultimate moment

4.2 Strain development and distribution

Figure 14 shows the development of strain in CFRP sheets and steel bars with increasing load. Both CFRP sheets strain and tensile steel bar strain exhibit a three-stage development: in the early stage, the strain rate increases slowly due to the beam not yet cracking; after concrete cracked, the curve undergoes a turning point, indicating that the CFRP sheets and the tensile steel rebar carry the tensile stress after the concrete released, and the strain increases significantly with the increasement of load. After the tensile steel rebar yielded, a second turning point appears. The steel rebar stress remains unchanged, and the CFRP sheets bear a larger tensile stress until the beam failed.

From the development of strain, it can also be seen that the cracking load and yield load of the test beam increase with the increasing of the prestrain of the CFRP sheets. The introduction of prestress can increase the crack resistance of the beams, reduce the strain of the tensile steel rebar under the same level of load, share the tensile stress of the steel rebar, and indirectly increase the yield load and ultimate load of the beams. However, for beams that experience end debonding failure, the ultimate load is significantly reduced, which limits the strength utilization of the CFRP material.

4.3 Model validation

Using the analytical method established in this paper, the cracking load, yield load, and ultimate load of the test beams were calculated. The measured prestresses of the CFRP

sheets under different prestressing methods are shown in Table 3. In the calculation, the measured value of prestress in the CFRP sheets was used to ensure the consistency of the initial conditions of prestress. The calculation results are shown in Table 4. It can be seen from the table that the average value and coefficient of variation of the ratio of experimental values to calculated ones for the cracking load are 1.14 and 0.05, respectively, for the yield load are 1.06 and 0.04, respectively, and for the ultimate load are 1.03 and 0.10, respectively. Overall, the calculated values are in good agreement with the experimental values and can be used to predict the bending performance of the RC beams strengthened with prestressed CFRP sheets under different prestressing methods.

5 Conclusions

An experimental work was conducted on the bending performance of RC beams strengthened with prestressed CFRP sheets using the prestressing methods of mechanical tensioning and the temperature-induced recovery of SMA wires. Based on the experimental results, a comprehensive analysis method for the entire bending process of the strengthened beams was proposed. The main conclusions are as follows:

1) During the yield and strengthening stages, the stress-strain hysteresis loops of SMA wires under cyclic loading-unloading were basically consistent for different prestrains. As the prestrain of the SMA wire increased, the maximum recovery stress also increased. When the prestrain of the SMA wire reached 10%, the maximum recovery stress reached 448.5 MPa. However, when the prestress was introduced into the CFRP sheets through temperature-induced recovery, under the same prestrain conditions, the maximum recovery stress decreased by 37.8–39.5%.
2) The failure mode of the prestressed CFRP sheets strengthened beams by mechanical tensioning was the debonding of the CFRP sheets caused by mid-span bending cracks, while the failure mode of the beams prestressed through the temperature-induced recovery of SMA wires was the end debonding of the CFRP sheets. Both methods of prestressing significantly improved the cracking moment and yield moment of the strengthened beams. However, the ultimate load of the strengthened beams prestressed through the temperature-induced recovery of SMA wires was only slightly increased due to premature peeling of CFRP sheets.
3) The mechanical tensioning prestressed CFRP sheets strengthened beam had a relatively large increase in stiffness, while the stiffness increase of the SMA wire prestressed beam through temperature-induced recovery was limited due to the gradual end debonding of the CFRP sheets. The prestress effect did not effectively limit the development of cracks. In the mechanical tensioning prestressed CFRP sheets strengthened beam, the strain of the CFRP sheets developed fully, and the CFRP sheets bore a large tensile stress, effectively limiting the development of cracks.
4) The present study proposes a comprehensive analysis method for the bending behavior of prestressed CFRP sheets strengthened beams. The calculated results are in good agreement with experimental results, indicating that the proposed method can be used to predict the bending performance of the strengthened beams.

Authors' contributions
Zhang Zhao-jun: Methodology and Conceptualization; Wang Wen-wei: Supervision; Zhen Jing-shui and Li Bo-cheng: Experiment; Cai De-cheng and Du Yang-yan: Review & Editing.

Funding
This study was financially supported by National Natural Science Foundation of China (Project No.51878156) and EPC Innovation Consulting Project for Longkou Nanshan LNG Phase I Receiving Terminal (Z2000LGENT0399).

Availability of data and materials
The data and materials in the current study are available from the corresponding author on a reasonable request.

Declarations

Competing interests
The authors declared no potential conflicts of interest with respect of to the research, authorship, and/or publication of this article.

Received: 30 January 2024 Accepted: 3 March 2024
Published online: 03 April 2024

References

Basaran B, Kalkan I (2020) Investigation on variables affecting bond strength between FRP reinforcing bar and concrete by modified hinged beam tests. Compos Struct 242:112185
Derkowski W, Walczak R (2021) Possibilities of increasing effectiveness of RC structure strengthening with FRP materials. Mater (Basel) 14(6):1387
Feng P, Lu XZ, Ye LP (2011) Application technology of fiber-reinforced composite materials in construction engineering. China Architecture & Building, Beijing
Frigione M, Lettieri M (2018) Durability issues and challenges for material advancements in FRP employed in the construction industry. Polymers 10(3):247
Hassan WM, Hodhod OA, Hilal MS, Bahnasaway HH (2021) Tests on FRP-retrofitted tension-controlled eccentric and biaxial high strength concrete columns. Compos Struct 276:114536
Hui YX, Xue YJ, Wang WW, Tan X (2022) FRP/SMA experimental study on mechanical performance and recoverable performance of Composite materials. J Compos Sci 39:1–15
Koteš P, Vavruš M, Jošt J, Prokop J (2020) Strengthening of concrete column by using the wrapper layer of fibre reinforced concrete. Materials 13(23):5432
Kueres S, Will N, Hegger J (2020) Shear strength of pre-stressed FRP reinforced concrete beams with shear reinforcement. Eng Struct 206:110088
Wang WW (2007) FRP strengthening technology and application of reinforced concrete structures. China Architecture & Building, Beijing
GB 50010-2010 (2010) Code for design of concrete structures [S]. China Architecture and Construction Press, Beijing
JTG 3362-2018 (2018) Specifications for Design of Highway Reinforced Concrete and Prestressed Concrete Bridges and Culverts [S]. China Communication Press, Beijing
Shi JZ (2021) Research progress on externally prestressed fiber-reinforced resin-based composite reinforced concrete structures. J Compos Sci 38(07):2092–2106
Soleilhet F, Quiertant M, Benzarti K (2023) Numerical modelling of the nonlinear shear creep behavior of FRP-Concrete Bonded joints. Materials 16(2):801
Teng JG, Yao J (2007) Plate end debonding in FRP-plated RC beams-II: strength model. Eng Struct 29(10):2472–2486
Tiwary AK, Singh S, Kumar R, Sharma K, Chohan JS, Sharma S, Singh J, Kumar J, Deifalla AF (2022) Comparative study on the behavior of reinforced concrete beam retrofitted with CFRP strengthening techniques. Polymers 14(19):4024
Wang WW, Dai JG, Harries KA (2013) Performance evaluation of RC beams strengthened with an externally Bonded FRP system under simulated vehicle loads. J Bridge Engineering 18(1):76–82
Wang WW, Dai JG, Harries KA, Bao QH (2012) Pre-stress losses and flexural behavior of reinforced concrete beams strengthened with posttensioned CFRP sheets. J Compos Constr 16(2):207–216
Xue Y-J, Cai D-C, Wang W-W, Tian J (2023) Jing-Shui Zhen, Bo-Cheng Li. Pre-stress loss and flexural behavior of precracked RC beams strengthened with FRP/SMA composites. Compos Struct 321:117319
Xue Y-J, Wang WW, Tan X, Hui YX, Tian J (2022) Zhong Feng Zhu. Mechanical behavior and recoverable properties of CFRP shape memory alloy composite under different pre-strains. Constr Build Mater 333:127186
Zhang L, Wang WW, Harries KA, Tian J (2015) Bonding behavior of Wet-Bonded GFRP-Concrete interface. J Compos Constr 19(6):04015001

Publisher's Note